Supporting Information

Controllable Size and Crystallinity of Ru Nanoparticles on Carbon Support by Fluidized Bed Reactor-Atomic Layer Deposition for Enhanced Hydrogen Oxidation Activity

Woo-Jae Lee,[a,b] Susanta Bera,[a,b] Hyun-Jae Woo,[b] Jung-Won An,[b] Jong-Seong Bae[c], Il-Kwon Oh[d] and Se-Hun Kwon,[a,b]*

[a]*Institute of Materials Technology, Pusan National University, 30 Jangjeon-Dong Geumjeong-Gu, Busan 46241, Republic of Korea*
[b]*School of Materials Science and Engineering, Pusan National University, 30 Jangjeon-Dong Geumjeong-Gu, Busan 46241, Republic of Korea*
[c]*Busan Center, Korea Basic Science Institute, Busan 46742, Republic of Korea*
[d]*Department of Electrical and Computer Engineering, Ajou University, 206 Worldcup-ro, Suwon 16499, Republic of Korea*

TABLE OF CONTENTS

◈ **Additional and detailed FBR-ALD process for synthesizing Ru catalyst**.

In the deposition process, carbon supports were inserted on the glass bead in the middle of reactor which contains a mesh structured support at the bottom, where reactions between carbon and precursor occur. Precursor and reactant were injected from bottom to upward direction through porous support of the carbon samples to make it fluidize continuously. However, fluidizing behavior can vary according to the characteristic of powder. According to the Gerdart's diagram, carbon black is very difficult to be fluidized due to the various range of agglomerated carbon black sizes. As an ideal condition to fluidize carbon blacks, cluster size-controlled of carbon within the range of 60-120 μm has been selected by filtering using the sieve being in the A group region categorized in Gerdart's diagram,[1] which is easy to fluidize the powders. Due to the strong van der waals bonding of the carbon black, it can be well fluidized without busting during deposition.

Before inserting carbon supporter into reactor, glass beads (1 mm) fill chamber to mesh height for well-fluidizing powder, which is positioned at the middle of reactor. The reactor with carbon black powder (0.4g) was evacuated by rotary pump to 0.01 torr slowly to avoid pumping powders out, which takes approximately 2 min to approach the base working pressure. Because of this, ALD system have 2 pumping line, consisting of narrow pumping line for slow pumping and wide line for deposition process.

◈ Citric acid treatment of the carbon supporter

For carbon black, citric acid treatment is implemented to maximize the functional groups of carbon support surface. Carbon black (20 g) was dipped into aqueous solution mixed with water 1L and citric acid 20 g. After stirring by spoon with hand, carbon black solution was more mixed by stirring the magnetic bar on stirrer for 1h at room temperature. Carbon black in solution was filtered through a paper filter and washed with DI-water until acid is removed, identifying it by PH paper. Filtered carbon black was heated into thermal furnace at 300 °C for 1h. To make sure the effect of the treatment, XPS analysis (**following Figure S1**) was conducted. The results indicate that O *1s* spectra of the carbon after acid treatment (**Figure S1 (b)**) possessed richer functional groups related to the oxygen than that before treatment (**Figure S1 (a)**).

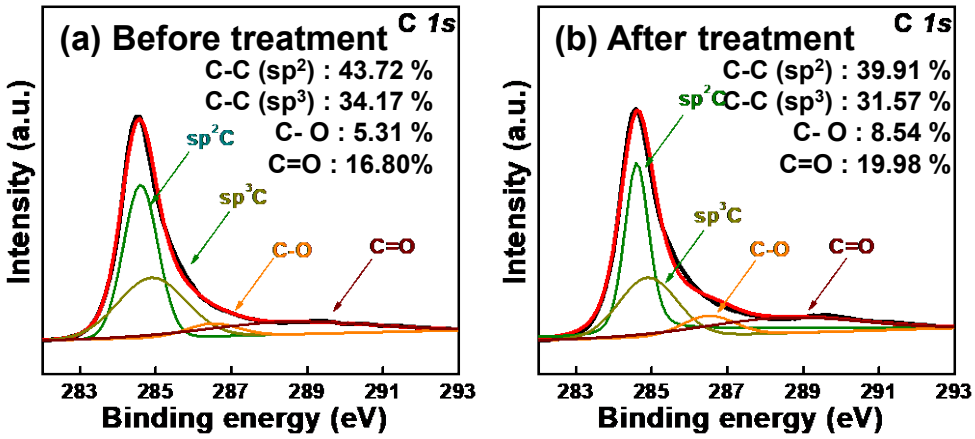

Figure S1. O *1s* XPS spectra and its deconvolution for the carbon supporter **(a)** before and **(b)** after acid treatment.

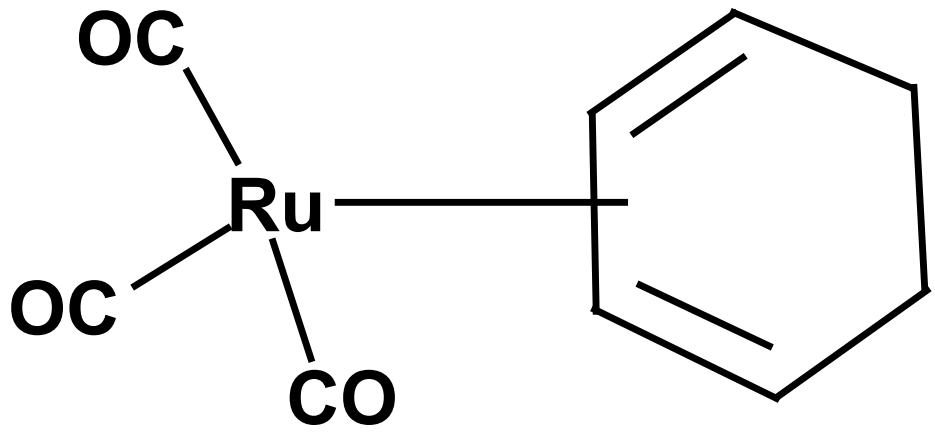

Figure S2. Molecular 2D structure of the Ru $(CO)_3(\eta^4\text{-}C_6H_8)$.

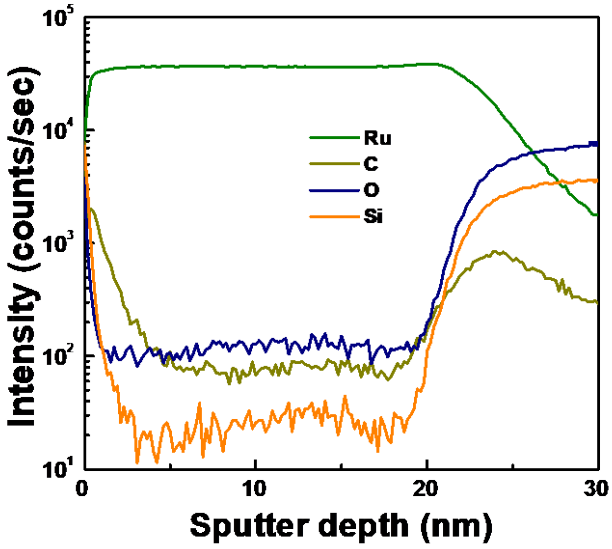

Figure S3. Depth profiling of SIMS for Ru thin film on SiO_2 wafer.

The carbon and oxygen peaks were almost similar with the Si background peak, indicating the low impurities within Ru thin film.

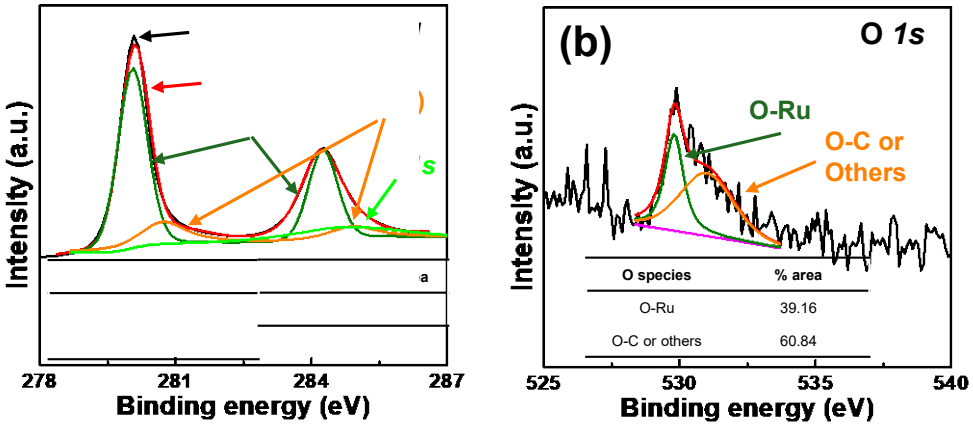

Figure S4. XPS deconvolution of **(a)** Ru *3d* and **(b)** O *1s* for Ru thin film on SiO_2 wafer.

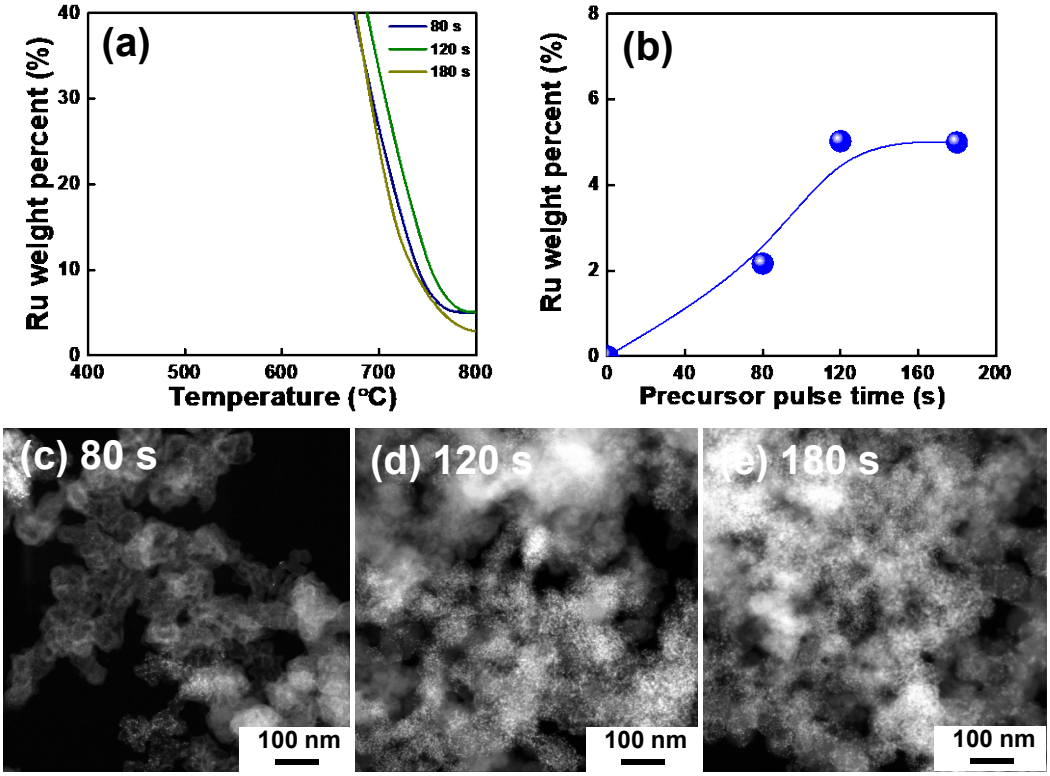

Figure S5. **(a)** TGA analysis and **(b)** Ru wt. % depending on the precursor pulse time, and STEM images of Ru catalysts for **(c)** 80 s, **(d)**120 s, and **(e)**180 s pulse time with 5 ALD cycles.

A precursor pulse time was varied from 80 to 180 s with 5 cycles on the carbon support when the enough reactant and carrier gas purge times were fixed at 90 s, 90 s and 90 s. Ru wt. % were calculated from TGA analysis, as shown in **Figure S5 (a)**. And the results were summarized in the **Figure S5 (b)**. It was shown that Ru loading was saturated above the 120s, indicating the self-limiting reaction, a nature characteristic of ALD. In addition, over than 120s (**Figure S5 (d) and R5 (e)**), uniform and well dispersed Ru NPs were observed compared to the non-optimized ALD process (**Figure S5 (c)**). This observation clearly indicates the growth of Ru on carbon is occurred by the typical self-limiting ALD growth mode.

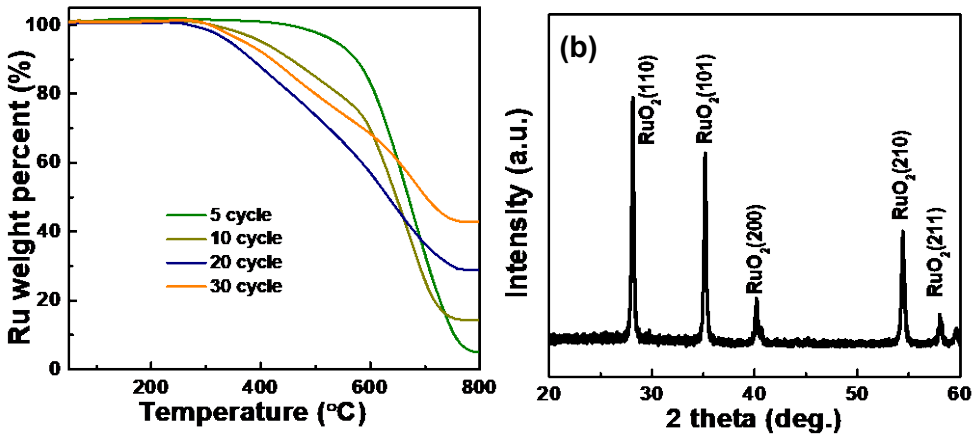

Figure S6. **(a)** TGA curve of the Ru/carbon catalyst. **(b)** XRD pattern of the residue after TGA test.

TGA was investigated under an air atmosphere. After burning the carbon to CO_2, Ru is converted to the RuO_2, which is confirmed by the XRD pattern from **Figure S6 (b)**. Based on the formula of RuO_2, 75.95 % of RuO_2 came from the Ru. From this, Ru wt. % can be calculated from the TGA analysis.[2]

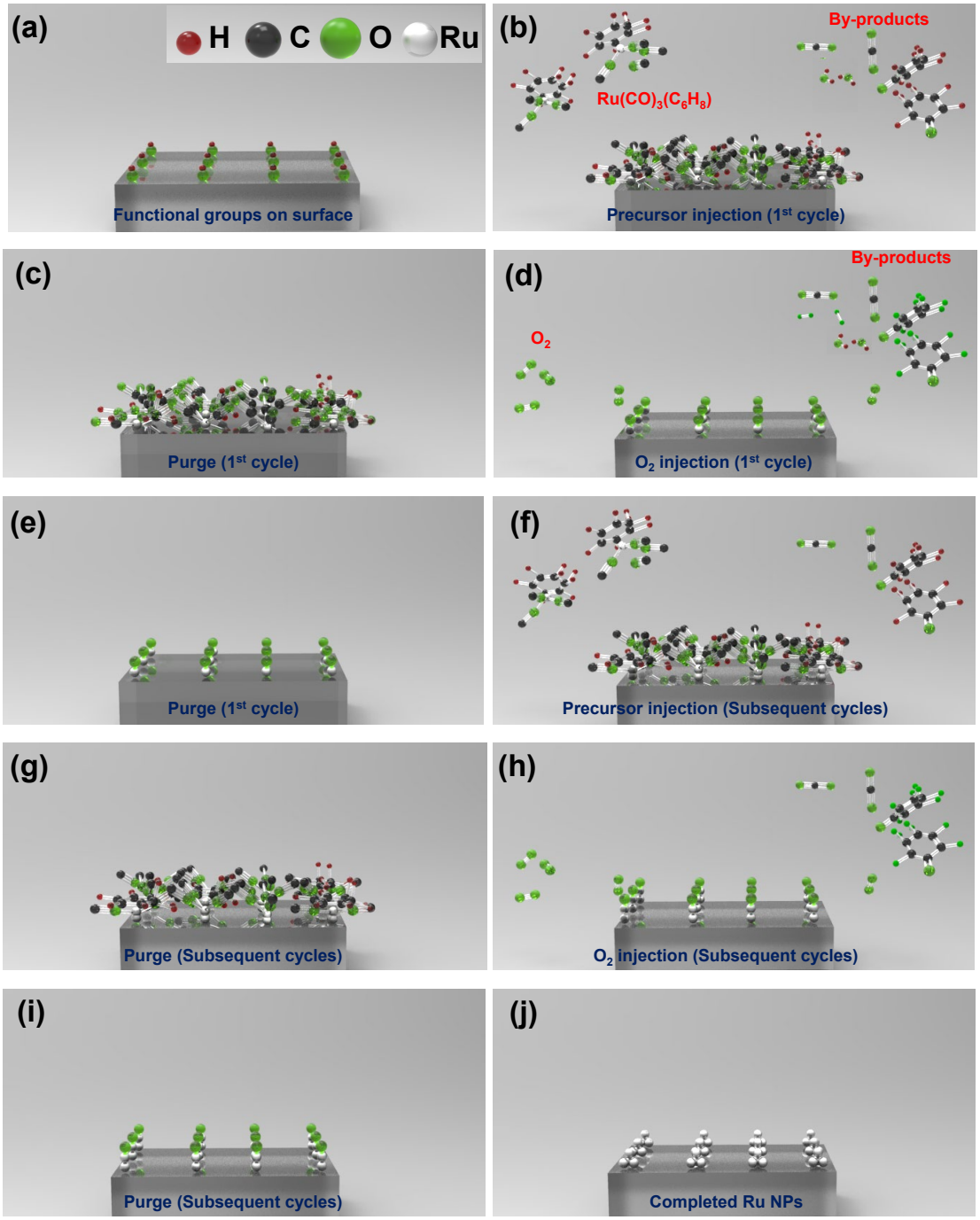

Figure S7. Schematic illustration for the proposed Ru-ALD process using Ru $(CO)_3(\eta^4\text{-}C_6H_8)$ and O_2 reactant: **(a)** before deposition, **(b)** precursor pulse, **(c)** purge, **(d)** O_2 pulse and **(e)** another purge for 1st cycle. For the subsequent cycles, **(f)** precursor pulse, **(g)** purge, **(h)** O_2 pulse and **(i)** another purge and **(j)** the completed ALD Ru NPs with the desired size by repeating the cycles.

Before deposition, the carbon surface was pretreated to maximize the function groups ((ex) -

OH) on its surface before the ALD process (**Figure S7 (a)**). During the ALD process, ALD cycle consisted of four steps; a precursor injection, a purge, a reactant injection, and another purge. During the precursor injection step of the 1st ALD cycle, Ru $(CO)_3(\eta^4\text{-}C_6H_8)$ could react with the terminated hydroxyl (-OH) functional groups on the carbon, followed by the formation and the purging out of the gaseous by-products probably such as H_2O, CO_2 and cyclohexanone (C_6H_8O), and the rest of the precursors would be chemically adsorbed on the surface (**Figure S7 (b)**). Increasing precursor injection time could produce the saturated chemisorbed precursor layer (less than one monolayer) at a certain time from which excess precursor (high concentration of precursor) cannot participate in the surface chemisorption reaction. The excess precursors and volatile by-products are purged except those which are already chemically adsorbed on the surface (**Figure S7 (c)**). In the next step, when the O_2 as a reactant is dosed, it could react with the chemisorbed precursor and combust the remaining ligands, producing the gaseous volatile by-products. In addition, some additional oxygen might dissociatively chemisorbs on the Ru surface, and this reactive O* atoms would remain chemisorbed until subsequent Ru precursor was exposed (**Figure S7 (d)**). During another purge step, all the gaseous volatile by-products and the excess O_2 gas were evacuated (**Figure S7 (e)**). After the 1st cycle, the Ru surface could be covered with reactive O* atoms, indicating that Ru-O* became the surface anchoring site of the regeneration from the 2nd cycle on. Therefore, during the Ru precursor pulse time, CO or C_6H_8 ligands in Ru $(CO)_3(\eta^4\text{-}C_6H_8)$ precursors could react with the surface "O*" through the combustion reaction, forming the gaseous CO_2 and cyclohexanone (C_6H_8O) by-products and the rest of the precursors are chemically absorbed (**Figure S7 (f)**). After that, the remaining growth mechanism would be the same as the rest processes (purge-O_2 injection-another purge) of the 1st cycle (**Figure S7 (g)-(i)**). This sequence (**Figure S7 (f)-(i)**) is repeated to obtain the desired Ru NP size (**Figure S7 (j)**).

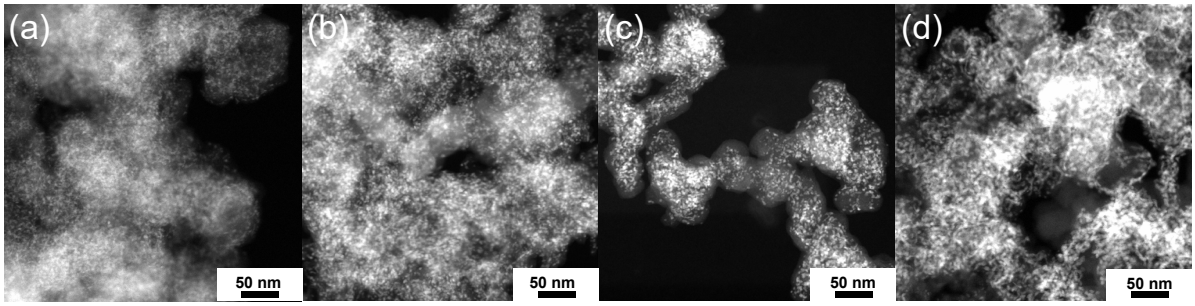

Figure S8. Low-magnified HAADF-STEM images of Ru catalysts as a function of cycles; **(a)** 5 cycles, **(b)** 10 cycles, **(c)** 20 cycles and **(d)** 30 cycles.

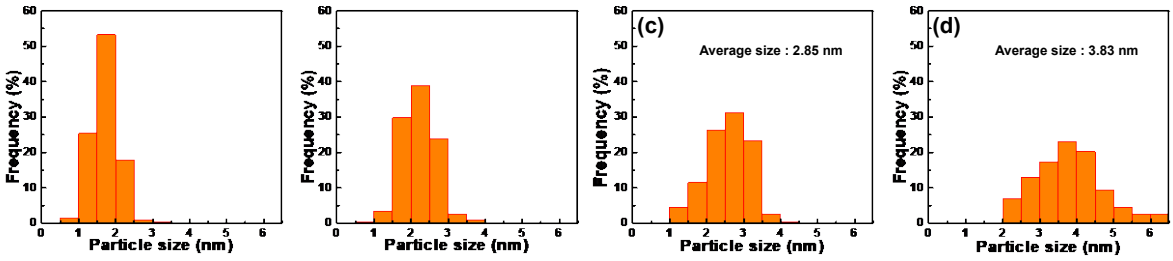

Figure S9. Particle size and distribution of Ru catalysts as a function of cycles; **(a)** 5 cycles, **(b)** 10 cycles, **(c)** 20 cycles and **(d)** 30 cycles.

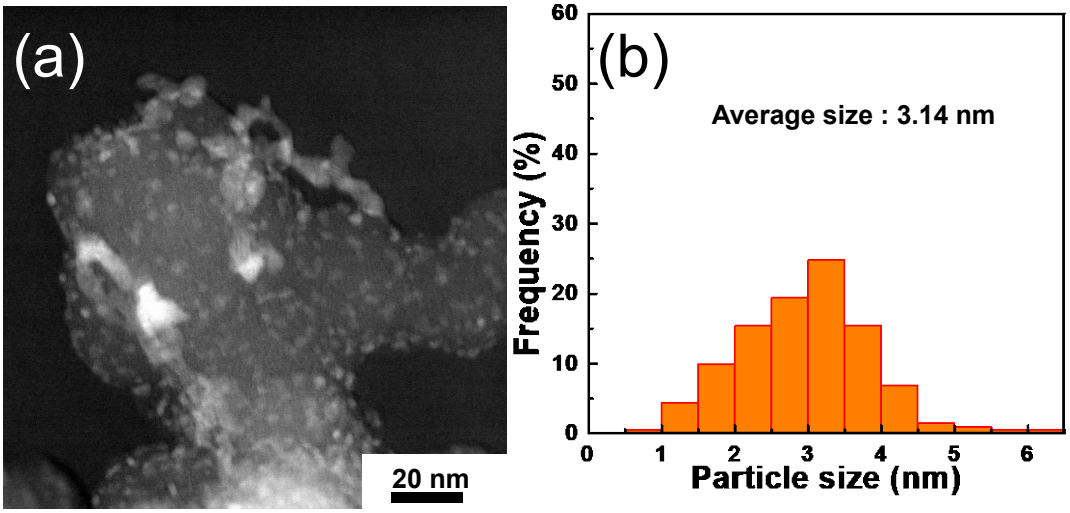

Figure S10. (a) HAADF-STEM images, and **(b)** Particle size and distribution of commercial Ru catalyst (Premetek, 20 wt. %).

For the particle size distribution, all the particle sizes were counted except for highly agglomerated NPs.

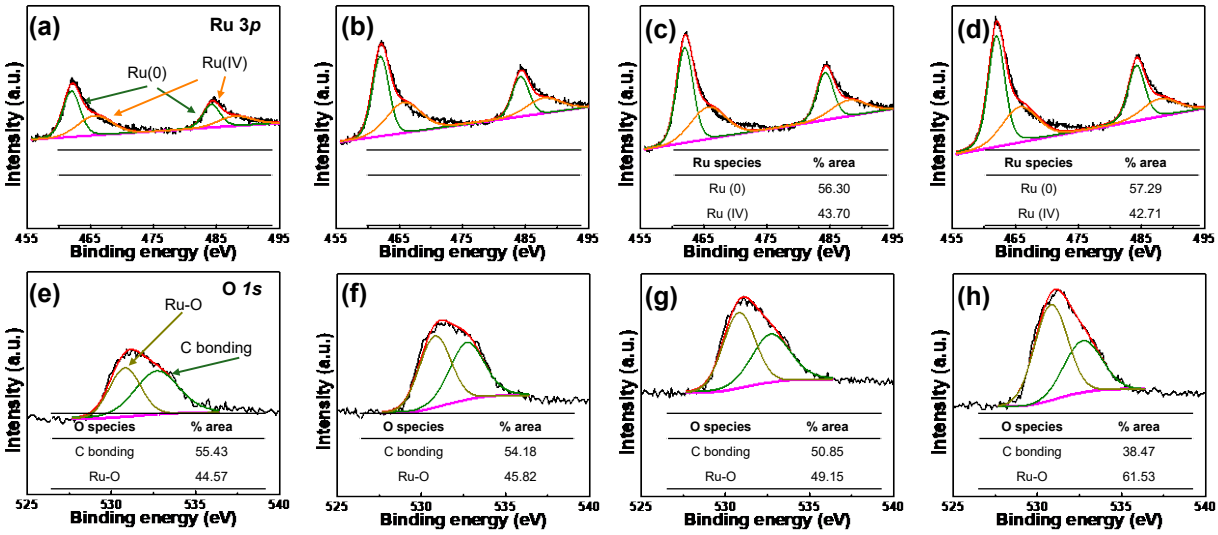

Figure S11. XPS deconvolution of Ru *3p* and O *1s* for Ru catalysts as a function of ALD cycles: **Figure (a), (e)** : 5 cycles, **Figure (b), (f)** : 10 cycles, **Figure (c), (g)** : 20 cycles and **Figure (d), (h)** : 30 cycles). **Figure (a)-(d)** presents Ru *3p* peak and **Figure (e)-(h)** shows O *1s* peak.

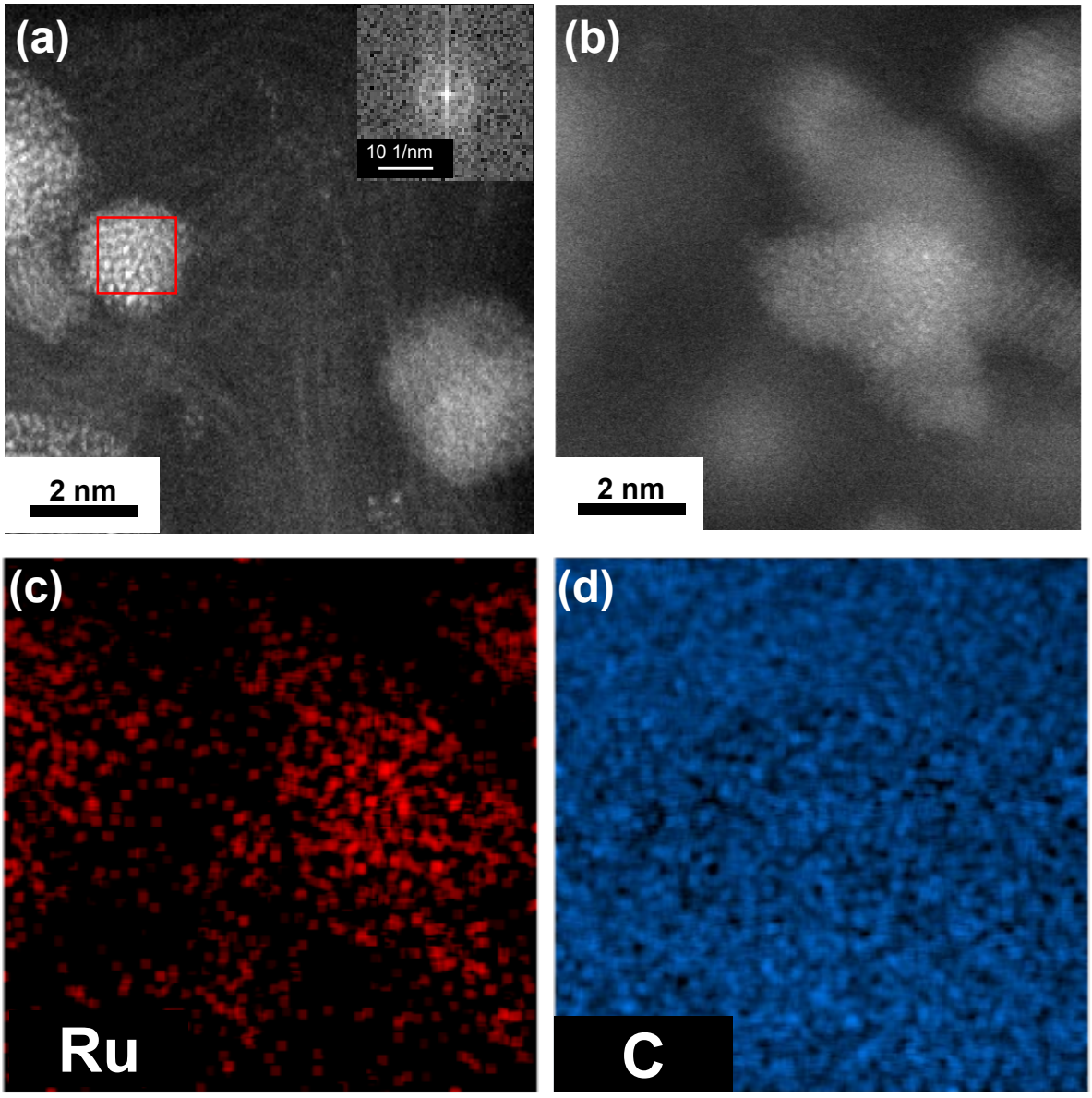

Figure S12. Cs-TEM and EDS mapping images of 5 cycled Ru catalyst

Cs-TEM images of 5 cycled Ru catalyst with less than 2nm NPs was shown in the **Figure S12 (a)**. Because NPs showed the amorphous structure as indicated by inset FFT, Ru catalyst is hard to be perceived. Therefore, another Cs-TEM image **(b)** was analyzed for EDS mapping with **(c)** Ru and **(d)** C elements.

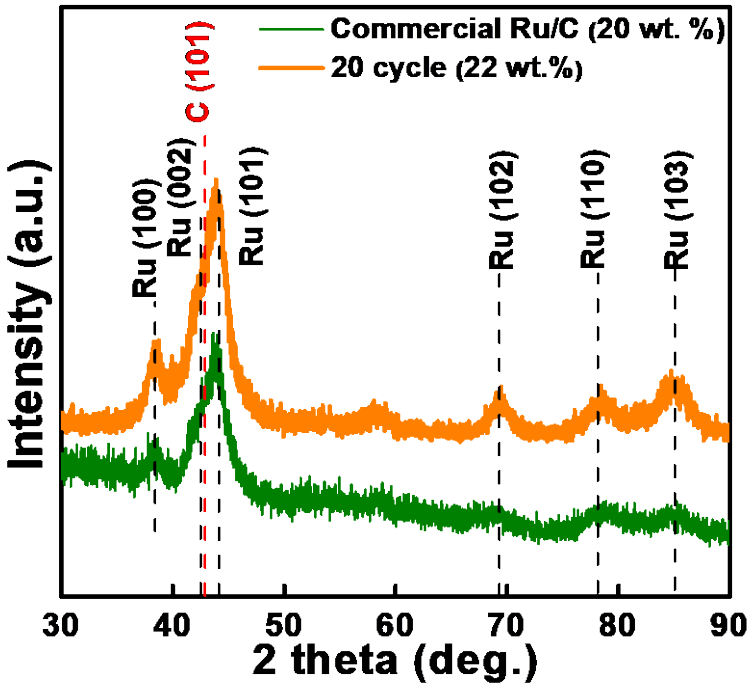

Figure S13. XRD spectra of ALD and commercial Ru catalysts with similar weight percent.

The Ru loadings of 20 cycled Ru catalyst and commercial Ru catalyst were 22 and 20 wt. %, respectively.

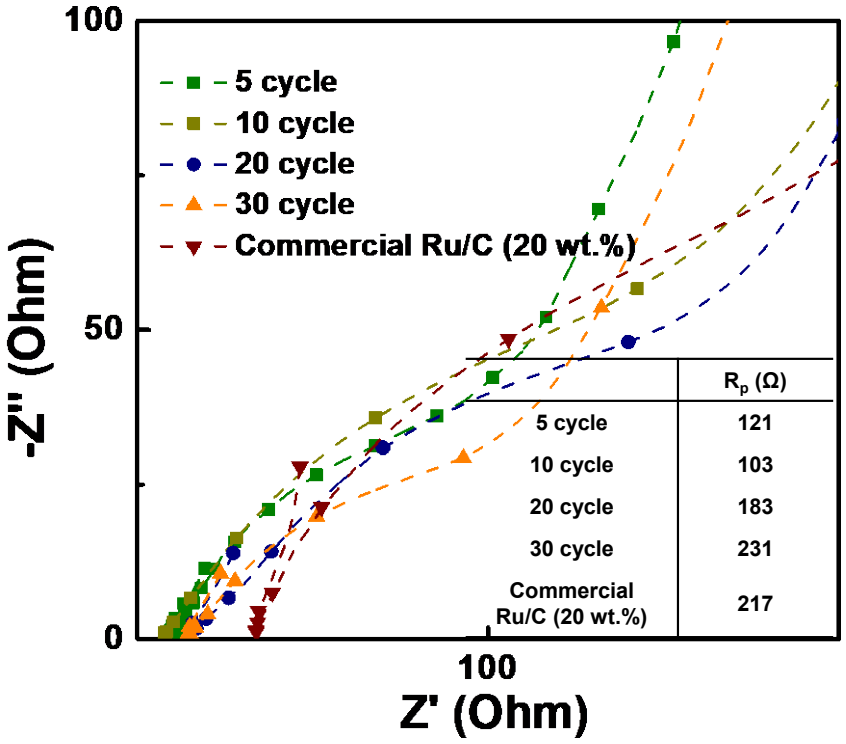

Figure S14. Electrochemical impedance spectroscopy (EIS) of Ru catalysts as a function of ALD cycles.

For the EIS analysis, it was performed at a DC potential of 0.05V, with an AC frequency range of 10k Hz-0.01 Hz and AC amplitude of 5mV.

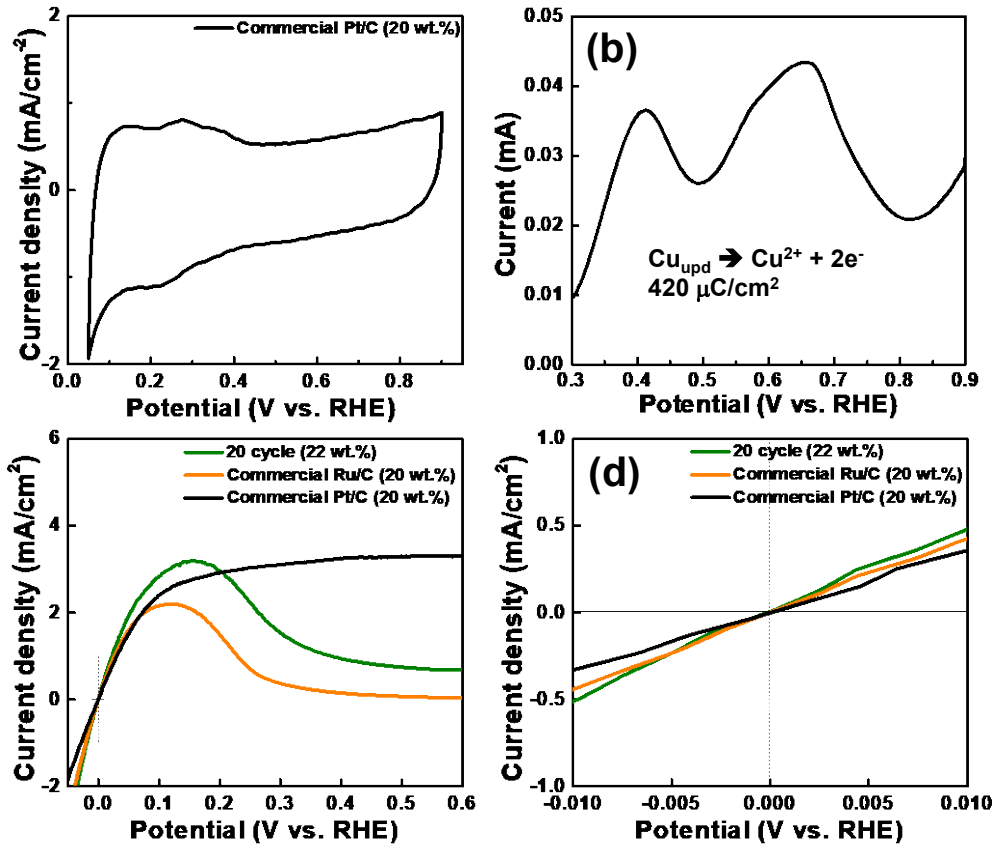

Figure S15. **(a)** Cyclic voltammetry, **(b)** Cu_{upd} stripping voltammograms, **(c)** polarization curve, and **(d)** low overpotential region of polarization curve of commercial Pt catalyst (Premetek, 20 wt. %).

Polarization curve of Pt catalyst was compared with Ru catalysts (ALD Ru catalyst and commercial Ru/C (Premetek, 20 wt. %)) with the similar metal wt. %.

Table S1. BET surface area of Ru catalysts as a function of ALD cycles.

Samples	BET surface area (m^2/g)
Bare	356.11
5 cycles	295.92
10 cycles	260.20
20 cycles	221.51
30 cycles	209.25

Table S2. Electrochemical surface area of Ru catalysts as a function of ALD cycles.

Samples	ECSA (m^2/g)
5 cycles	174.70
10 cycles	149.71
20 cycles	117.68
30 cycles	111.15
Commercial Ru/C (20 wt.%)	102.51

Table S3. The comparison of ECSA, MA and SA for HOR at alkaline atmosphere. [3]

Sample	ECSA (m^2/g)	Mass activity (A/mg_{metal})	Specific activity (mA/cm^2_{metal})	Ref
FBR-ALD Ru/C	149.7	0.092	0.089	Present work
		0.275 (After iR-correction)	0.184 (After iR-correction)	Present work
Ru/C	131	0.082	0.063	[3]
Pt/C	119	0.060	0.05	[3]
Pd-CN_x	63	~0.018	0.034	[4]
Pd/C	78	~0.031	0.04	[5]
Pd/C-400C	-	0.04	0.062	[6]
Pd/C-CeO_2	-	0.024	0.054	[7]
PdIr/C	8.1	0.079	0.98	[8]
Ni/N-CNT	-	-	0.028	[2]

Table S4. MA, SA, and hydrogen binding energy of Pt catalyst (Premetek, 20 wt. %).

Sample	Mass activity (A/mg_{Pt})	Specific activity (mA/cm^2_{Pt})	Hydrogen binding energy (eV)
Pt catalyst	0.045	0.052	0.489

[1] Geldart D. *Powder Technol.* **1973**, *7*, 285-292.

[2] Zhuang Z.; Giles S. A; Zheng J.; Jenness G. R.; Caratzoulas S.; Vlachos D. G. *Nature Comm.* **2016**, 7, 10141 (8p).

[3] Xiao Q.; Lei W.; Wang J.; Gao G.; Zhao T.; Cordeiro M. A. L.; Lin R.; Gong M.; Guo X.; Stavotski E.; Xin H. L.; Wang D. *J. Mater. Chem. A* **2018**, 6, 11346-11352.

[4] Ohyama J.; Sato T.; Yamamoto Y.; Arai S.; Satsuma A. *J. Am. Chem. Soc.* **2013**, 135, 8016-8021.

[5] Bhowmik T.; Kundu M. K.; Barman S. *ACS Catal.* **2016**, 6, 1929-1941.

[6] Zheng J.; Sheng W.; Zhuang Z.; Xu B.; Yan Y. *Sci. Adv.* **2016**, 2, e1501602

[7] Zheng J.; Zhou S.; Gu S.; Xu B.; Yan Y. *J. Electrochem. Soc.* **2016**, 163, F499‑F506.

[8] Miller H.A.; Lavacchi A.; Vizza F.; Marelli M.; Di Benedetto F.; D'Acapito F.; Paska Y.; Page M.; Dekel D.R. *Angew. Chem. Int. Ed.* **2016**, 55, 6004-6007.

[9] Jervis R.; Mansor N.; Gibbs C.; Murray C.A.; Tang C.C.; Shearing P.R.; Dan J.L.B.; *J. Electrochem. Soc.* **2014**, 161, F458‑F463.